STUDIA UBB CHEMIA, LX, 4, 2015 (p. 173-184)
(RECOMMENDED CITATION)

CORROSION RESISTANCE OF LASER CLADDED NiCrBSi COMPOSITE COATINGS

IOSIF HULKA[a*], V.A. SERBAN[a], D. UTU[a], NARCIS DUTEANU[a*], A. PASCU[b], I.C. ROATĂ[b]

ABSTRACT. NiCrBSi powders were deposited on medium alloy steel substrate using laser cladding process and electrochemically tested at room temperature by immersing the specimens in 3.5% NaCl solution in order to study their corrosion behavior. The coatings were obtained using different cladding parameters like scanning speed and overlap percentage. Investigations techniques such as scanning electron microscopy (SEM), energy dispersive X-ray spectroscopy (EDS), potentiodynamic polarization and electrochemical impedance spectroscopy (EIS) measurements were employed to study the microstructure and chemical properties of the coatings. It was found that the microstructural characteristic and corrosion behavior are linked to coatings thickness, dilution and diffusion of Fe within the coating.

Keywords: *laser cladding, powders, coatings, corrosion, NiCrBSi;*

INTRODUCTION

Laser cladding, is one of the surface modification technologies widely employed for deposition of protective coating on cheaper substrate or materials with poor wear and corrosion resistance like carbon steel [1]. The process uses lasers as a concentrated heat source to manufacture coatings with a very good metallurgical bond with the substrate. The coatings are meant to increase the lifetime of different components by preventing them from severe wear and corrosion [2]. The process is superior to other deposition methods like hard-facing in terms of feedstock material consumption, high productivity and low distortion. During cladding, a melt pool is formed on the substrate by the laser beam while it scans the surface and the filler material, which usually is a

[a] *Politehnica University of Timisoara, Piaţa Victoriei Nr. 2, 300006 Timişoara, Romania*
[b] *Transilvania University of Brasov, Materials Engineering and Welding Department, 29 Eroilor Blvd., 500036, Brasov, Romania*
** Corresponding authors: hulka_iosif@yahoo.com, narcis.duteanu@upt.ro*

powder or wire, is addend and fused to the substrate. During the process, high heating and rapid cooling rates occurs resulting fine microstructures and metastable phases during solidification [3]. If the cooling rate is too fast, the melt-pool solidifies rapidly, and crack formation might occur which is a major drawback for laser cladding. Cracking is detrimental to the corrosion behavior of the coatings because they act as sites for crevice and pitting corrosion [4].

Ni-based self-fluxing alloys are mainly used in petro-chemical industry, glass industry and others for applications as mud purging elements, hot working punches, fan blades, earth working machine elements, etc. [5]. Their advantages are related to easy coating of large sized components.

NiCrBSi is one of the alloys used in laser cladding to enhance wear and corrosion resistance at moderate and elevate temperatures. Si and B, present in the filler material, increase the self-fluxing capabilities of the alloy, improving the ability to obtain depositions by melting process. The role of Cr is to improve the mechanical properties as a consequence of its combination with other elements to produce hard precipitates [6].

The aim of the present research was to investigate the influence of different deposition parameters such as scanning speed and overlapping percentage of laser tracks on the microstructure, hardness and also their influence on corrosion behavior, in a 3.5% NaCl solution at room temperature, on the obtained NiCrBSi laser cladded coatings.

RESULTS AND DISCUSSION

Powder Characterization

Figure 1a shows spherical powder particles with surface dimples caused by the collision of particles during atomization. In cross-section (Fig. 1b) the powder consists of fine cellular and dendritic microstructures. Some pores might be noticed as well. The powder composition (Fig. 1c) determined by EDS analysis confirm the chemical elements presented in Table 2.

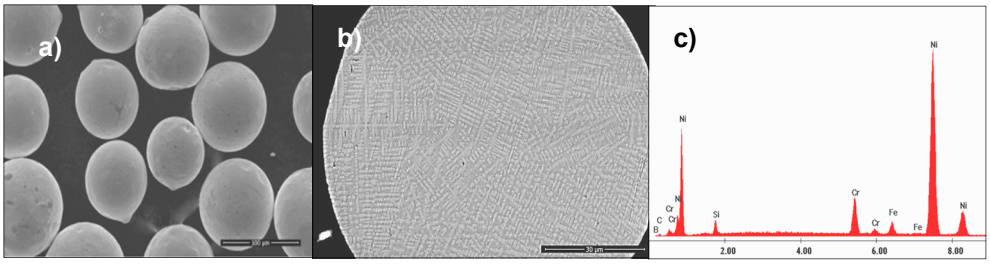

Figure 1. SEM image of (a) NiCrBSi gas atomized powder particles, (b) cross-section of powder particle and (c) EDS analysis of powder

Coating Microstructure and Chemical Composition

The optical micrographs (OM) of the coatings (Fig. 2) revealed a good adhesion between the cladded material and substrate, indicating that the powder was melted complete and sufficiently. All of the coatings exhibit dense structure with reduced porosity. Depending on the deposition parameters, presented in Table 1, different coating thicknesses were obtained, thus influencing the dilution process. At lower overlapping areas and higher deposition speed growth the coatings were thinner.

The dilution, present in the laser cladded coatings, quantifies the relative amount of substrate material molted during the deposition process and mixed with molten material from the new cladded coating. In order to obtain high quality cladded coatings some dilution is required between the substrate and cladded coating to ensure a good metallurgical bond. Even if the dilution it is required, it must stay low otherwise it may degrade the coating properties [7].

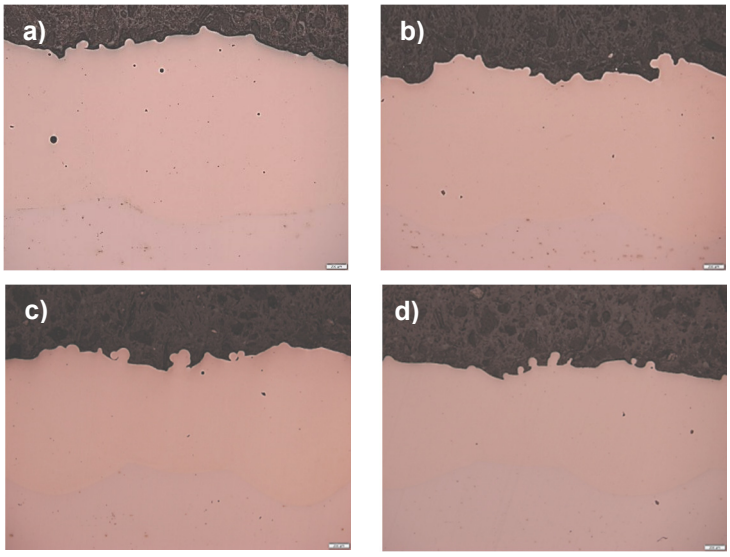

Figure 2. OM of laser cladded coatings (a) Sample 1; (b) Sample 2; (c) Sample 3; (d) Sample 4.

Figure 3a illustrates the etched microstructure, the chemical composition being revealed by the EDS spectrum (Fig. 3b). For all sample the morphology of the NiCrBSi coatings was similar. The matrix phase consists from a solid solution of Ni with Cr and Fe providing a dendritic structure. Between the dendritic structures an intermetallic laminar eutectic phase is present. The microstructure and chemical composition of the laser cladded coatings is similar to results presented by authors for similar alloys [8].

Dilution in a thicker laser cladded coating formed by overlapping can be expected to be smaller because part of the beam energy is consumed in order to melt the overlapped track [7], this being a reason why in present study the thicker the coating the smaller the dilution is.

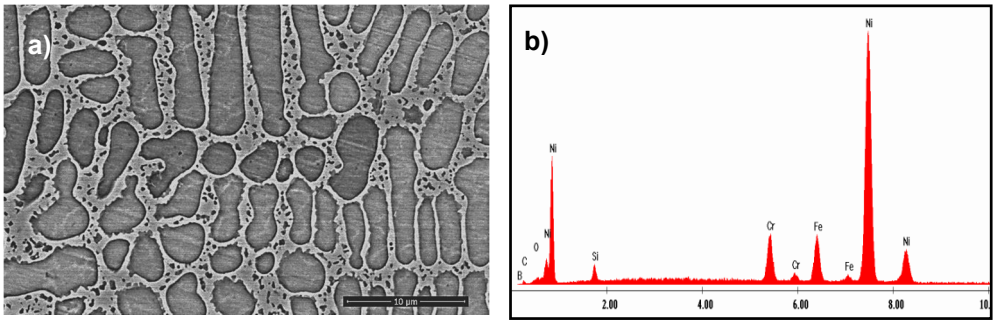

Figure 3. Close-up SEM of NiCrNSi laser cladded coating of the dendritic structure (a) and EDS analysis (b).

Results of micro-hardness measurements, thickness and porosity of coatings are presented in Table 1. Hardness measurements were performed along a straight line in all the laser cladded coatings. The average hardness value of the coatings decreased as the coating became thinner because of the Fe diffusion from the substrate that was melted. The thicknesses of the coatings differ, depending of their different deposition parameters like scanning speed and overlap percentage, thus Sample 1 is the thickest. The reduced amount of porosity, less than 1%, indicated dense and compact coatings. Small differences between the values might be attributed due to different deposition angles.

Table 1. Micro-hardness and coating thicknesses

Sample	$Hv_{0.3}$	Thickness [mm]	Porosity %
1	431.8 ± 11.2	1.81 ± 0.19	0.67 ± 0.92
2	408.8 ± 20.3	1.43 ± 0.23	0.06 ± 0.05
3	407.4 ± 21.2	1.21 ± 0.21	0.55 ± 0.66
4	376.1 ± 37.5	0.98 ± 0.18	0.03 ± 0.03

The chemical compositions of different areas, in cross-section of the coatings, were studied as it is indicated in Figure 4 in the upper (a), middle (b) and lower (c) part of the coating and as well in the coating-substrate interface (d). The results are summarized in Table 4. Boron could not be detected clearly in the EDS quantification due to its relatively low atomic mass and it was not included in the analysis as well as oxygen and carbon.

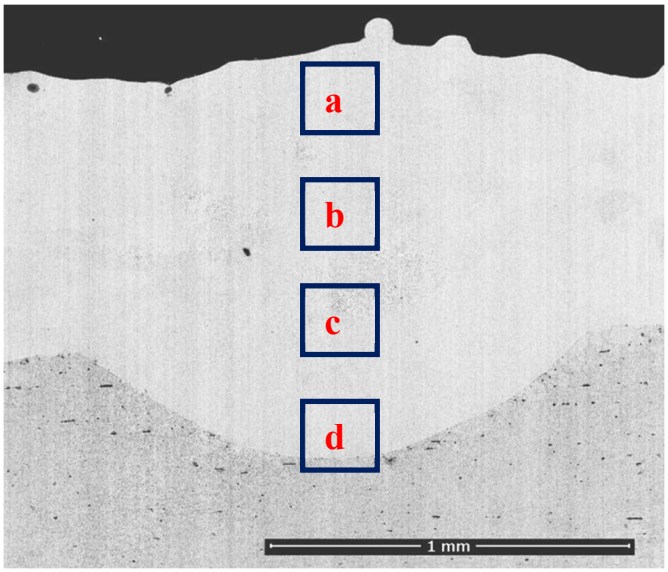

Figure 4. SEM of laser cladded NiCrBSi coating indicating EDS areas of interest

It might be noticed that the Ni, Cr and Si content is more concentrated in the upper part of the coating while this values changed, reaching lower values at the coating-substrate interface while Fe content proved the opposite. This is might be due to diffusion process from the substrate. The high temperature reached during the cladding process may have also been contributed to the Fe diffusion.

Table 2. EDX quantification results

	Sample 1				**Sample 2**			
El. wt%	**a**	**b**	**c**	**d**	**a**	**b**	**c**	**d**
Ni	68.58	67.2	66.83	35.5	67.56	67.01	65.15	34.67
Cr	9.71	7.98	8.17	2.44	8.44	7.39	7.29	2.25
Si	13.54	14.54	13.08	7.93	14.55	13.54	14.09	5.20
Fe	8.17	10.29	11.91	54.0	9.45	12.05	12.66	57.89
	Sample 3				**Sample 4**			
El. wt%	**a**	**b**	**c**	**d**	**a**	**b**	**c**	**d**
Ni	63.9	63.04	60.83	33.03	65.63	64.16	58.2	35.33
Cr	7.85	7.7	6.76	2.38	8.88	7.87	6.41	2.87
Si	17.68	18.27	14.61	16.11	20.09	14.84	15.57	8.42
Fe	10.57	10.99	17.8	55.91	5.40	13.13	19.82	53.38

Corrosion Tests

Potentiodynamic polarization studies

Potentiodynamic polarization curves of NiCrBSi laser cladded coatings are shown in Figure 5. Prior to start the corrosion tests all coatings were ground and polished to the same roughness in order to allow similar testing conditions to avoid differences which might affect the test results.

According to obtained linear polarization curves at room temperature, the parameters values like corrosion rate, corrosion current density (i_{corr}), corrosion potential (E_{corr}) in conformity with Tafel slopes associated with anodic (b_a) and cathodic (b_c) processes, were determined by extrapolating the linear part of recorded curves using GPES software.

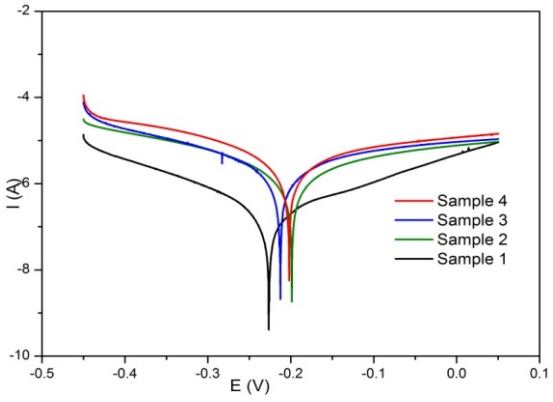

Fig. 5. Potentiodynamic polarization curves for laser cladded NiCrBSi coatings in 3.5% NaCl solution at 22°C

Linear polarization curves recorded for laser cladded coatings are presented in Figure 5. It is possible to calculate the polarization resistance from the linear polarization curves by using Stern and Geary equation [9] and the corrosion rate can be then calculated based on Faraday's Law [10] and the obtained data is presented in Table 3. Analyzing the data it might be noticed that the current density and corrosion rate corresponding for the corrosion process is lower for Sample 1 and higher for Sample 4.

Table 3. Corrosion parameters calculated from the polarization curves with 28.82 [g] equivalent weight and 8.14 [g/cc] density values

Sample	icorr. [A]	Ecor. [V]	Corr. Rate [mm/year]
1	2.021E-7	-225	1.853E-3
2	1.542E-6	-372	1.413E-2
3	1.357E-6	-416	1.245E-2
4	2.708E-6	-353	2.484E-2

This can be explained by the higher coating thickness and reduced Fe dissolution compared to the other coatings, which makes the material nobler.

Electrochemical Impedance Spectroscopy EIS

The Niquist plot depicted in Figure 6 shows the presence of a semi-circle – depressed capacitive loop at high to intermediary frequencies range [11], followed by an almost linear dependence which is associated with a mixed kinetic and diffusion control of the process [5]. Presence of the capacitive loop can be associated with the charge transfer resistance and appear from time constant of electrical double layer [11, 12].

Analyzing the EIS spectra presented in Figure 6 can observe that the semi-circle diameter is increasing in order sample 1, sample 2, sample 3 and sample 4. Deviation from the perfect circular shape observed in recorder EIS spectra was generally attributed to electrode superficial inhomogeneity and also to the mass transport resistance [13, 14]. Also, this inhomogeneity can be associated with different interfacial phenomena or with surface toughness [13]. Electrochemical theory express that the first intersection with x axis represents the solution resistance and the second one is associated with the charge transfer resistance (semicircle diameter). It is expected that the corrosion resistance is increase when the charge transfer resistance increase.

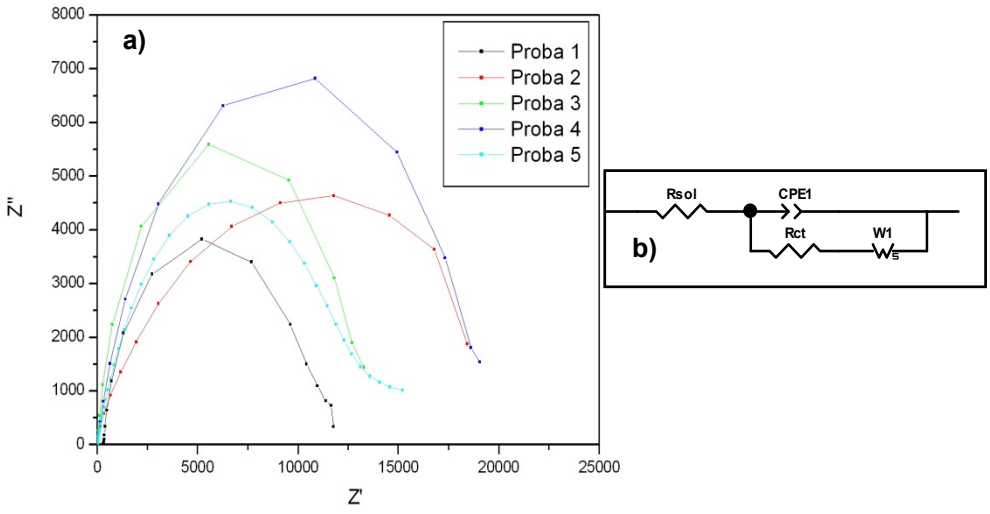

Figure 6. Niquist plot (a) and equivalent circuit for spectra modelation (b)

Parameters associated with corrosion process were obtained by modeling the recorded impedance spectra using the electrical equivalent circuit presented in Figure 6b which describe the metal / electrolyte interface.

Equivalent circuit used is represented by a serial connection of solution resistance with a constant phase element (CPE) which is in parallel with a charge transfer resistance connected in series with a Warburg impedance. Usage of this Warburg element can be associated with mass transport process and suggests that the studied corrosion process is limited by mass transport [15]. In same time, CPE represent a modified capacitance describe by equation:

$$Z_{CPE} = {}^{1}\!\!\diagup\!\!_{Y_0}\,(j\omega)^n \tag{1}$$

where Y_0 represent one parameter which can be related with the double layer capacitance, and n represent an exponent between 0 and 1 describing the constant phase angle of CPE [12].

Considering the case of a finite length thickness of the diffusion layer δ, can describe the impedance of Warburg element using the equation 2 [16]:

$$Z_w = (R_w(jw\tau_D)^{-\theta})tanh(jw\tau_D)^{-\theta} \tag{2}$$

Rw – diffusion resistance; τ_D – diffusion time constant given by $\tau_D = \delta^2/D$, where δ – diffusion thickness and D – diffusion coefficient; φ – an exponent whit values between 0 and 1.

Based on R_s, R_{ct} and CPE values can calculate the double layer capacity using equation 3 [11]:

$$C_{dl} = \left[\frac{T}{\left(\frac{1}{R_S} - \frac{1}{R_{ct}}\right)^{1-n}}\right]^{1/n} \tag{3}$$

In Table 4 are listed the values of electrochemical impedance parameters obtained by CNLS fitting of experimental data.

Analyzing data presented in Table 4 can observe that the charge transfer resistance is increasing in order: sample 1, sample 2, sample 3, sample 4, which can be associated with increase of corrosion resistance in same order. Also, it can be observed that all of the samples have reduced porosity, suggesting that the corrosion mechanism is similar in all 4 cases. Decrease of C_{dl} value, in same order, suggests that the number of active sites presented on the surface of the samples is increasing.

Table 4. Electrochemical impedance parameters obtained by CNLS fitting of experimental data

Sample	Resistances [Ω cm^{-2}]		CPE1		W			C_{dl}
	R_{sol}	R_{ct}	Y_0 [F cm^{-2} S^n]	n (0 – 1)	R_w [Ω cm^{-2}]	τ_D [s]	φ	C_{dl} [μF cm^{-2}]
1	15.2	12204	1.5919E-5	0.90985	0.254	6.7223E-4	0.23924	6.98
2	12.95	12989	2.6328E-5	0.92386	0.00145	2.3366E-7	0.38522	6.01
3	15.5	18101	4.1223E-5	0.62274	0.164	0.2338	0.06002	6.00
4	15.15	19853	2.5589E-5	0.83775	5.472E-4	1.1394E-7	0.38637	5.59

CONCLUSIONS

The influence of scanning speed and overlap percentage on the properties and corrosion behavior of NiCrBSi laser cladded coatings, from commercial feedstock powder, was studied.

From the experimental results, the following conclusions can be drawn:

Using laser cladding process and NiCrBSi powder, dense and almost pore-free coatings might be manufactured with different microstructural characteristics due to different deposition parameters.

According to EDS quantification and due to diffusion process, the Fe content decreases from top of the coatings to interface, reaching higher values at the coating-substrate interface, while for the other elements exactly the opposite occurs.

The hardness of the coating decreases slightly as the coatings becomes thinner, due to dilution process.

The corrosion test indicated that the thicker coating (Sample 1) due to higher overlapping percentage of laser tracks (60%) is nobler and presents better corrosion behavior.

EXPERIMENTAL SECTION

Coating deposition

Laser cladding has been carried out using a Coherent 1000F diode laser and a Precitec YC50 water cooled cladding module manipulated by a CLOOS welding robot. The laser beam is in infrared field with a wavelength of 975 nm and a maximum divergence of 56 mm*mrad. The powder was provided to the cladding head with AT-1200HPHV Termach feeding system and Argon gas was used for shielding and carrier of the powder. The influence of scanning speed and overlap percentage on coatings properties was investigated. The cladding parameters used in the present study are presented in Table 5.

Powder characterization

The used cladding material is a Metco 12 C gas-atomized nickel based self fluxing powder with nominal size in the range of -125+53 μm, the relevant characteristics are presented in Table 6.

The powders morphology and microstructure was studied by scanning electron microscopy (SEM) equipped with energy dispersive X-ray (EDX) micro-analyzer.

Table 5. Cladding parameters

	Laser power [W]	Power density [kW/cm^2]	Speed [cm/min]	Powder feed rate [g/min]	OverlapPercent [%]
Sample 1	780	24.8	16	5	60
Sample 2	780	24.8	20	5	50
Sample 3	780	24.8	24	5	45
Sample 4	780	24.8	30	5	40

Table 6. Chemical composition in wt% of NiCrBSi feedstock powder

Powder	Supplier	Trade name	Chemical properties	Ni %	Cr %	B %	Si %	Fe %	C %
NiCrBSi	Sulzer Metco	Metco 12 C		Balance	10	2,5	2,5	2,5	0,15

Coatings characterization

The samples were metallographically prepared by using abrasive papers and polishing clothes with diamond suspension. Coatings microstructures were evaluated by means of optical microscopy, scanning electron microscopy (SEM), and energy dispersive X-ray analysis (EDX). Cross-section images of the samples were taken by an Olympus optical microscope and the SEM images with a Quanta FEG 250 (FEI, The Netherlands) equipped with EDAX analyzer. An Olympus Vickers micro-hardness tester was employed to ascertain the micro-hardness of the laser cladded coatings under a 300 gf load.

Corrosion tests

Electrochemical tests were performed at room temperature with an Autolab 302 N potentiostat/galvanostat using a 100 ml cell equipped with three electrodes: working electrode consisting of NiCrBSi laser cladded samples, Ag/AgCl reference electrode and a platinum mesh used as counter electrode. For the experiments the exposed surface of specimens were 1 cm^2, submerged and kept in a 3.5 wt.% NaCl solution (synthetic sea water) for 30 min to achieve the equilibrium. After the equilibrium was reached the polarization curves were

recorded using GPES software in order to evaluate the corrosion rate. All linear polarization curves were recorded in the potential range ± 250 mV versus open circuit potential at a scan rate of 0.5 mV s^{-1}. Electrochemical Impedance Spectroscopy (EIS) data were recorded using the FRA (Frequency Response Analyzer) module. All EIS experiments were performed at E_{corr} after 30 min equilibrium time, when the stationary stage were reached in frequency range 100 KHz to 100 mHz. Recorded EIS data were modelled with ZView software using a complex non-linear procedure (CNLS). Measurements were carried out in aerated solution at room temperature.

ACKNOWLEDGEMENTS

This work was supported by the strategic grant POSDRU/159/1.5/S/ 137070 (2014) of the Ministry of Labour, Family and Social Protection, Romania, co-financed by the European Social Fund – Investing in People, within the Sectoral Operational Programme Human Resources Development 2007-2013.

REFERENCES

[1]. X. Lou, L. Li, G.J.Li, *Journal of Alloys and Compounds,* **2015**, *626*, 102.
[2]. P. Nie, O.A. Ojo, Z. Li, *Surface and coatings Technology*, **2014**, *258*, 1048.
[3]. A. Ray, K. S. Arora, S. Lester, M. Shone, *Journal of Materials Processing Technology*, **2014**, *214*, 1566.
[4]. S. Zhou, Y. Huang, X. Zeng, Q. Hu, *Material Science and Engineering A*, **2008**, *480*, 564.
[5]. N. Serres, F. Hlawka, S. Costil, C. Langlade, F. Machi, *Journal of Materials Processing Technology*, **2011**, *211*, 133.
[6]. T.G-del Rio, M.A. Garrido, J. E. Fernandez, M. Cadenas, J. Rodrigues, *Journal of Materials Processing Technology*, **2008**, *204*, 304.
[7]. U. de Oliveira, V. Ocelik, J.Th.M. De Hosson, *Surface and Coatings Technology*, **2005**, *197*, 127.
[8]. T.E. Abioye, D.G. McCartney, A.T. Clare, *Journal of Material Processing Technology*, **2015**, *217*, 232.
[9]. Princetown Applied Research, Application note CORR1 *http://www.princetonapplied.*
[10]. Stansbury, E.E.; Buchenan, R.A., Fundamentals of electrochemical corrosion, published by ASM Int., Mater. Park, Ohio, **2000**, ISBN 0871706768.
[11]. H. Ashassi-Sorkhabi, N. Ghalebsaz-Jeddi, F. Hashemzadeh, H. Jahani, *Electrochimica Acta*, **2006**, *51*, 3848.

[12]. Application note – Gamry instruments, http://www.gamry.com/application-notes/basics-of-electrochemical-impedance-spectroscopy/
[13]. A. Lecante, F. Robert, P.A. Blandinieres, C. Roos, *Current Applied Physics*, **2011**, *11*, 714.
[14]. K.F. Khaled, M*aterial Chemistry and Physics*, **2008**, *112*, 290.
[15]. E.M. Sherif, Su-Moon Park, Electrochimica Acta, **2006**, *51*, 1313.
[16]. M. Dan, N. Vaszilcsin, A. Kellenberger, N. Duteanu, *Studia UBB Chemia,* **2011**, *1*, 119.